

$K^0\Lambda$ photoproduction off the neutron with nucleon resonancesSang-Ho Kim^{1,*} and Hyun-Chul Kim^{2,3,4,†}¹*Asia Pacific Center for Theoretical Physics (APCTP), Pohang 37673, Republic of Korea*²*Department of Physics, Inha University, Incheon 22212, Republic of Korea*³*Advanced Science Research Center, Japan Atomic Energy Agency, Shirakata, Tokai, Ibaraki, 319-1195, Japan*⁴*School of Physics, Korea Institute for Advanced Study (KIAS), Seoul 02455, Republic of Korea*

(Dated: November 8, 2021)

We investigate kaon photoproduction off the neutron target, i.e., $\gamma n \rightarrow K^0\Lambda$, focusing on the role of nucleon resonances given in the Review of Particle Data Group in the range of $\sqrt{s} \approx 1600 - 2200$ MeV. We employ an effective Lagrangian method and a Regge approach. The strong couplings of nucleon resonances with $K\Lambda$ vertices are constrained by quark model predictions. The numerical results of the total and differential cross sections are found to be in qualitative agreement with the recent CLAS and FOREST experimental data. We discuss the effects of the narrow nucleon resonance $N(1685, 1/2^+)$ on both the total and differential cross sections near the threshold energy. In addition, we present the results of the beam asymmetry as a prediction.

Keywords: $K^0\Lambda$ photoproduction, effective Lagrangian approach, t -channel Regge trajectories, nucleon resonances.

arXiv:1806.01992v2 [hep-ph] 20 Sep 2018

* E-mail: sangho.kim@apctp.org

† E-mail: hchkim@inha.ac.kr

1. Kuznetsov et al. reported the measurement of the cross sections for η photoproduction off the neutron, which shows a narrow bump structure near the center-of-mass (CM) energy $W = 1.68$ GeV [1]. In the $\gamma p \rightarrow \eta p$ reaction, there is only a small dip structure at the same energy. The LNS-KEK Collaboration [2], the CB-ELSA and TAPS Collaborations in Bonn [3], and the A2 Collaboration in Mainz [4–6] have confirmed this feature of η photoproduction off the neutron. This phenomena is often called the *neutron anomaly* in η photoproduction. However, there is no consensus in the interpretations on the narrow enhancement at $W = 1.68$ GeV. In fact, the narrow nucleon resonance around 1.68 GeV was predicted by the chiral quark-soliton model [7–11] in which the neutron anomaly was explained in terms of the different values of the $N(1685) \rightarrow N\gamma$ transition magnetic moments. The A2 measurement of the helicity-dependent $\gamma n \rightarrow \eta n$ cross sections favors the existence of a narrow P_{11} resonance [4]. On the other hand, Ref. [12, 13] disputed that such the narrow enhancement arises from the interference between $N(1535, 1/2^-)$ and $N(1650, 1/2^-)$, based on the Bonn-Gatchina multi-channel partial-wave analysis. However, Ref. [14] refuted it in favor of the narrow P_{11} nucleon resonance. In this situation it is of great importance to scrutinize the narrow structure around 1.68 GeV and the related neutron anomaly in other processes such as $K^0\Lambda$ photoproduction.

In the present Letter, we investigate the $K^0\Lambda$ photoproduction off the neutron, focussing on the effects of the narrow resonance structure around 1.68 GeV, which appeared in the $\gamma n \rightarrow \eta n$ reaction. Since the threshold energy of the $\gamma n \rightarrow K^0\Lambda$ is 1.61 GeV, $K^0\Lambda$ photoproduction can provide a possible clue in understanding the nature of the narrow nucleon resonance $N(1685, 1/2^+)$. In this regard, the investigation on $K^0\Lambda$ photoproduction will shed light on the neutron anomaly yet from the different facet. While the theoretical investigations of $\gamma n \rightarrow \eta n$ reaction have been carried out extensively in the literature [15–19], that of $K^0\Lambda$ photoproduction is very limited [20–23]. Recently, the FOREST Collaboration at the Research Center for Electron Photon Science, Tohoku University [24, 25] and the CLAS Collaboration at the Thomas Jefferson National Accelerator Facility [26] have announced the experimental data on the total and differential cross sections of $K^0\Lambda$ photoproduction off the neutron¹. Very recently, the beam-target helicity asymmetry E is also measured at the CLAS Collaboration [27]. Thus, it is of great interest to examine theoretically the role of the narrow nucleon resonance $N(1685, 1/2^+)$ also in this $\gamma n \rightarrow K^0\Lambda$ reaction. We will employ an effective Lagrangian approach in which we can consider directly the nucleon resonances in the s channel. We will introduce sixteen different nucleon resonances up to 2.2 GeV. In addition, we take into account the narrow nucleon resonance $N(1685, 1/2^+)$ corresponding to the narrow enhancement found in η photoproduction off the neutron. We also include the K^* Reggeon exchange in the t channel, since it explains properly the high-energy behavior of the total cross section.

2. In an effective Lagrangian approach, the $\gamma n \rightarrow K^0\Lambda$ reaction can be represented by the tree-level Feynman diagram illustrated in Fig. 1. The notations of the four momenta of the incoming and outgoing particles are given in Fig. 1(a) in which the t -channel K^* Reggeon exchange is depicted. Other exchanges such as $K_1(1270, 1^+)$, $K_1(1400, 1^+)$, and higher strange mesons are excluded in the present process because of their small photocouplings to the K^0 meson, e.g., $\text{Br}(K^*(1410, 1^-) \rightarrow K^0\gamma) < 2.2 \times 10^{-4}$ [28].

The s -channel diagrams shown in Fig. 1(b) include contributions from the neutron and their resonances, generically. We will consider the sixteen different nucleon resonances taken from the Particle Data Group (PDG) data [28]. On top of them, we include the narrow resonance $N(1685, 1/2^+)$, which corresponds to the narrow enhancement found in η photoproduction [1–6]. Λ and Σ exchanges are included in the u -channel diagrams drawn in Fig. 1(c).

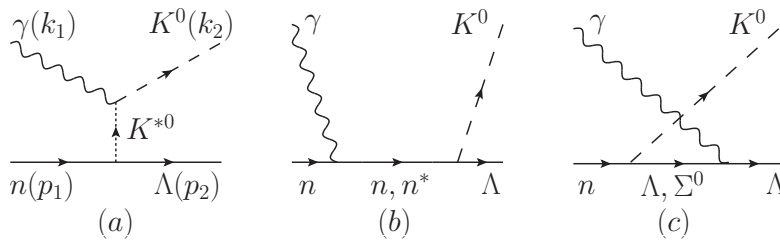


FIG. 1. Feynman diagrams for the $\gamma n \rightarrow K^0\Lambda$ reaction.

The general expressions of the electromagnetic (EM) interaction Lagrangians can be written as

$$\mathcal{L}_{\gamma K K^*} = g_{\gamma K K^*}^0 \epsilon^{\mu\nu\alpha\beta} \partial_\mu A_\nu (\partial_\alpha \bar{K}_\beta^{*0} K^0 + \bar{K}^0 \partial_\alpha K_\beta^{*0}),$$

¹ However, one should keep in mind that both the experimental data from the CLAS and FOREST Collaborations were taken from the deuteron target, certain effects from the Fermi motion are involved in the course of extracting the two-body experimental data.

$$\begin{aligned}
\mathcal{L}_{\gamma NN} &= -\bar{N} \left[e_N \gamma_\mu - \frac{e\kappa_N}{2M_N} \sigma_{\mu\nu} \partial^\nu \right] A^\mu N, \\
\mathcal{L}_{\gamma\Lambda\Lambda} &= \frac{e\kappa_\Lambda}{2M_N} \bar{\Lambda} \sigma_{\mu\nu} \partial^\nu A^\mu \Lambda, \\
\mathcal{L}_{\gamma\Sigma\Lambda} &= \frac{e\mu_{\Sigma\Lambda}}{2M_N} \bar{\Sigma}^0 \sigma_{\mu\nu} \partial^\nu A^\mu \Lambda + \text{H.c.},
\end{aligned} \tag{1}$$

where A_μ , K , K^* , and N designate the fields for the photon, pseudoscalar kaon, vector kaon, and nucleon, respectively. Λ and Σ denote respectively the fields for the ground-state hyperons. M_N and e_N stand respectively for the mass and electric charge of the nucleon, whereas e denotes the unit electric charge. Since the neutron is involved in the present work, we need only the magnetic term in the γNN vertex.

Concerning the values of the coupling constants, $g_{\gamma K K^*}^0$ is determined by the experimental data for the decay width $\Gamma(K^* \rightarrow K\gamma)$, resulting in -0.388 GeV^{-1} [28]. The sign of the coupling is fixed from the quark model. The anomalous and transition magnetic moments of the baryons are given by the PDG [28]

$$\kappa_N = -1.91, \quad \kappa_\Lambda = -0.61, \quad \mu_{\Sigma\Lambda} = 1.61. \tag{2}$$

The effective Lagrangians for the meson-nucleon-hyperon interactions are given by

$$\begin{aligned}
\mathcal{L}_{K^*N\Lambda} &= -g_{K^*N\Lambda} \bar{N} \left[\gamma_\mu \Lambda - \frac{\kappa_{K^*N\Lambda}}{M_N + M_\Lambda} \sigma_{\mu\nu} \Lambda \partial^\nu \right] K^{*\mu} + \text{H.c.}, \\
\mathcal{L}_{KNY} &= \frac{g_{KNY}}{M_N + M_Y} \bar{N} \gamma_\mu \gamma_5 Y \partial^\mu K + \text{H.c.},
\end{aligned} \tag{3}$$

where Y represents generically the fields for the hyperons (Λ or Σ^0). The strong coupling constants are taken from the average values of the Nijmegen soft-core potential (NSC97) [29]

$$\begin{aligned}
g_{K^*N\Lambda} &= -5.19, \quad \kappa_{K^*N\Lambda} = 2.79, \\
g_{KN\Lambda} &= -15.5, \quad g_{KN\Sigma} = 4.70.
\end{aligned} \tag{4}$$

Note that although we use the pseudovector coupling for the latter one in Eq. (3), the numerical results of the present work almost do not change when the pseudoscalar coupling is employed, since the effects of nucleon and hyperon exchanges turn out to be tiny.

In general, the invariant amplitude for photoproduction can be written by

$$\mathcal{M}_h = I_h \bar{u}_\Lambda \mathcal{M}_h^\mu \epsilon_\mu u_N, \tag{5}$$

where ϵ_μ represents the polarization vector of the incident photon. u_N and u_Λ denote the Dirac spinors for the incoming nucleon and the outgoing Λ , respectively. The isospin factors are given by $I_{K^*} = I_N = I_\Lambda = 1$ and $I_\Sigma = -1$ in the present process. The effective Lagrangians of Eqs. (1) and (3) being considered, the individual amplitudes for the Born term are obtained as follows:

$$\begin{aligned}
\mathcal{M}_{K^*}^\mu &= \frac{g_{\gamma K K^*}^0 g_{K^*N\Lambda}}{t - M_{K^*}^2} \epsilon^{\mu\nu\alpha\beta} \left[\gamma_\nu - \frac{i\kappa_{K^*N\Lambda}}{M_N + M_\Lambda} q_t^\lambda \sigma_{\nu\lambda} \right] k_{1\alpha} k_{2\beta}, \\
\mathcal{M}_N^\mu &= \frac{e\kappa_N}{2M_N} \frac{g_{KN\Lambda}}{2M_N} \frac{1}{s - M_N^2} \gamma_\alpha \gamma_5 (\not{q}_s + M_N) \sigma^{\mu\nu} k_{1\nu} k_2^\alpha, \\
\mathcal{M}_\Lambda^\mu &= \frac{e\kappa_\Lambda}{2M_N} \frac{g_{KN\Lambda}}{M_N + M_\Lambda} \frac{1}{u - M_\Lambda^2} \sigma^{\mu\nu} k_{1\nu} (\not{q}_u + M_\Lambda) \gamma_\alpha \gamma_5 k_2^\alpha, \\
\mathcal{M}_\Sigma^\mu &= \frac{e\mu_{\Sigma\Lambda}}{2M_N} \frac{g_{KN\Sigma}}{M_N + M_\Sigma} \frac{1}{u - M_\Sigma^2} \sigma^{\mu\nu} k_{1\nu} (\not{q}_u + M_\Sigma) \gamma_\alpha \gamma_5 k_2^\alpha,
\end{aligned} \tag{6}$$

where $q_{t,s,u}$ designate the four momenta of the exchanged particles, i.e., $q_t = k_2 - k_1$, $q_s = k_1 + p_1$, and $q_u = p_2 - k_1$.

Considering the finite sizes of hadrons, we need to introduce a form factor at each vertex. It is of course well known that certain ambiguities arise from the selection of hadronic form factors, in particular, when higher spin resonant baryons are involved [30, 31]. Bearing in mind that most approaches based on effective Lagrangians inevitably contain uncertainties related to types of the form factors chosen, we will use the following generic type for the s and u -channel background diagrams

$$F_B(q^2) = \left[\frac{\Lambda_B^4}{\Lambda_B^4 + (q^2 - M_B^2)^2} \right]^2, \tag{7}$$

where q^2 denotes the squared momentum of $q_{s,u}$ and M_B the mass of the corresponding exchanged baryon B , respectively. The form factor given in Eq. (7) tames sufficiently unphysically increasing cross sections as W increases. However, the gaussian-type form factors, which will be discussed after Eq. (20), are employed for higher-spin baryon resonances, because they control more efficiently the resonance contributions such that the cross sections are regulated and the resonance structures are revealed reasonably well.

Although we are mainly interested in the vicinity of the threshold energy for $K^0\Lambda$ photoproduction, future experiments are expected to cover higher energy regions. Thus, we employ the t -channel Regge trajectory for the K^* -meson exchange and follow Refs. [32, 33]. This can be done by replacing the Feynman propagator in Eq. (6) with the Regge one as

$$\frac{1}{t - M_{K^*}^2} \rightarrow P_{K^*}^{\text{Regge}}(t) = \left(\frac{s}{s_0}\right)^{\alpha(t)-1} \frac{\pi\alpha'}{\sin[\pi\alpha(t)]} \left\{ e^{-i\pi\alpha(t)} \right\} \frac{1}{\Gamma[\alpha(t)]}, \quad (8)$$

where either a constant phase (1) or a rotating one ($e^{-i\pi\alpha(t)}$) can be considered for the Regge phase. The K^* Regge trajectory reads [33]

$$\alpha(t) = \alpha_{K^*}(t) = 0.83t + 0.25, \quad (9)$$

and $\alpha' \equiv \partial\alpha(t)/\partial t$ denotes the slope parameter. The energy-scale parameter is chosen to be $s_0 = 1 \text{ GeV}^2$ for simplicity. Consequently, the entire Born amplitude is written as

$$\mathcal{M}_{\text{Born}} = \mathcal{M}_{K^*}(t - M_{K^*}^2)P_{K^*}^{\text{Regge}}(t) + \mathcal{M}_n^{\text{mag}} F_n(s) + \mathcal{M}_\Lambda F_\Lambda(u) + \mathcal{M}_\Sigma F_\Sigma(u). \quad (10)$$

Unlike the charged kaon production, all the terms are manifestly gauge-invariant, so we do not need to introduce any prescription for gauge invariance.

We also introduce N^* contributions in the s channel. Among the nucleon resonances listed in the PDG, we take into account sixteen different nucleon resonances in the range of $\sqrt{s} \approx (1600 - 2200) \text{ MeV}$ [28], including the narrow $N(1685, 1/2^+)$ in addition. We first express the effective Lagrangians for the EM transitions of the nucleon resonances

$$\begin{aligned} \mathcal{L}_{\gamma NN^*}^{1/2^\pm} &= \frac{eh_1}{2M_N} \bar{N}\Gamma^\mp \sigma_{\mu\nu} \partial^\nu A^\mu N^* + \text{H.c.}, \\ \mathcal{L}_{\gamma NN^*}^{3/2^\pm} &= -ie \left[\frac{h_1}{2M_N} \bar{N}\Gamma_\nu^\pm - \frac{ih_2}{(2M_N)^2} \partial_\nu \bar{N}\Gamma^\pm \right] F^{\mu\nu} N_\mu^* + \text{H.c.}, \\ \mathcal{L}_{\gamma NN^*}^{5/2^\pm} &= e \left[\frac{h_1}{(2M_N)^2} \bar{N}\Gamma_\nu^\mp - \frac{ih_2}{(2M_N)^3} \partial_\nu \bar{N}\Gamma^\mp \right] \partial^\alpha F^{\mu\nu} N_{\mu\alpha}^* + \text{H.c.}, \\ \mathcal{L}_{\gamma NN^*}^{7/2^\pm} &= ie \left[\frac{h_1}{(2M_N)^3} \bar{N}\Gamma_\nu^\pm - \frac{ih_2}{(2M_N)^4} \partial_\nu \bar{N}\Gamma^\pm \right] \partial^\alpha \partial^\beta F^{\mu\nu} N_{\mu\alpha\beta}^* + \text{H.c.}, \end{aligned} \quad (11)$$

where the spin and parity are given in superscripts. N^* , N_μ^* , $N_{\mu\alpha}^*$, and $N_{\mu\alpha\beta}^*$ stand for the spin-1/2, -3/2, -5/2, and -7/2 nucleon-resonance fields, respectively, with

$$\Gamma^\pm = \begin{pmatrix} \gamma^5 \\ I_{4 \times 4} \end{pmatrix}, \quad \Gamma_\nu^\pm = \begin{pmatrix} \gamma_\nu \gamma^5 \\ \gamma_\nu \end{pmatrix}. \quad (12)$$

h_i designate the EM transition coupling constants and can be calculated from the Breit-Wigner helicity amplitudes A_i given in the PDG. We refer to Refs. [34, 35] for the explicit relations between them. It is found that the values of the A_i for the 2018 edition of Review of Particle Physics [28] are almost the same as those for the 2016 edition [36] except for the $N(1650, 1/2^-)$. It is changed from -50 ± 20 to $-10 [10^{-3}/\sqrt{\text{GeV}}]$. We want to mention that we use the data on $N(1650, 1/2^-)$ taken from the previous edition whereas those on excited nucleons are employed from the updated 2018 edition of PDG. All the relevant values are tabulated in Table I, where we adopt the central values of A_i . The electromagnetic coupling of the narrow resonance $N(1685, 1/2^+)$ is taken from Ref. [37]. As for the full decay width, the resonances less than 1800 MeV have rather small values ($\simeq 130 \text{ MeV}$) compared to those of the higher ones that give 200 – 400 MeV [28]. In the present numerical calculation, we use the values in parentheses in Table I.

TABLE I. The sixteen nucleon resonances listed by the Particle Data Group (PDG) [28] and information on their electromagnetic couplings. The helicity amplitudes $A_{1/2, 3/2}$ [$10^{-3}/\sqrt{\text{GeV}}$] are obtained from Ref. [28]. In addition, we introduce the narrow nucleon resonance in the last row of this Table, which corresponds to the narrow enhancement in η photoproduction [1–6].

State	Rating	Width [MeV]	$A_{1/2}$	$A_{3/2}$	h_1	h_2
$N(1650, 1/2^-)$	****	100-150(125)	-50 ± 20 [36]	...	-0.31	...
$N(1675, 5/2^-)$	****	130-160(145)	-60 ± 5	-85 ± 10	4.88	5.45
$N(1680, 5/2^+)$	****	100-135(120)	≈ 30	≈ -35	-7.44	8.57
$N(1700, 3/2^-)$	***	100-300(200)	25 ± 10	-32 ± 18	-1.43	1.64
$N(1710, 1/2^+)$	****	80-200(140)	-40 ± 20	...	0.24	...
$N(1720, 3/2^+)$	****	150-400(250)	-80 ± 50	-140 ± 65	1.50	1.61
$N(1860, 5/2^+)$	**	300	21 ± 13	34 ± 17	0.28	1.09
$N(1875, 3/2^-)$	***	120-250(200)	10 ± 6	-20 ± 15	-0.55	0.54
$N(1880, 1/2^+)$	***	200-400(300)	-60 ± 50	...	0.31	...
$N(1895, 1/2^-)$	****	80-200(120)	13 ± 6	...	0.067	...
$N(1900, 3/2^+)$	****	100-320(200)	0 ± 30	-60 ± 45	0.29	-0.56
$N(1990, 7/2^+)$	**	100-320(200)	-45 ± 20	-52 ± 27	6.92	7.54
$N(2000, 5/2^+)$	**	300	-18 ± 12	-35 ± 20	-0.47	-0.56
$N(2060, 5/2^-)$	***	300-450(400)	25 ± 11	-37 ± 17	0.027	-2.87
$N(2120, 3/2^-)$	***	260-360(300)	110 ± 45	40 ± 30	-1.71	2.41
$N(2190, 7/2^-)$	****	300-500(400)	-15 ± 13	-34 ± 22	-1.57	-0.62
$N(1685, 1/2^+)$		30			-0.315 [37]	

The effective Lagrangians for the strong interactions are written as

$$\begin{aligned}
\mathcal{L}_{K\Lambda N^*}^{1/2^\pm} &= -ig_{K\Lambda N^*} \bar{K} \bar{\Lambda} \Gamma^\pm N^* + \text{H.c.}, \\
\mathcal{L}_{K\Lambda N^*}^{3/2^\pm} &= \frac{g_{K\Lambda N^*}}{M_K} \partial^\mu \bar{K} \bar{\Lambda} \Gamma^\mp N_\mu^* + \text{H.c.}, \\
\mathcal{L}_{K\Lambda N^*}^{5/2^\pm} &= \frac{ig_{K\Lambda N^*}}{M_K^2} \partial^\mu \partial^\nu \bar{K} \bar{\Lambda} \Gamma^\pm N_{\mu\nu}^* + \text{H.c.}, \\
\mathcal{L}_{K\Lambda N^*}^{7/2^\pm} &= -\frac{g_{K\Lambda N^*}}{M_K^3} \partial^\mu \partial^\nu \partial^\alpha \bar{K} \bar{\Lambda} \Gamma^\mp N_{\mu\nu\alpha}^* + \text{H.c.}
\end{aligned} \tag{13}$$

The strong coupling constants, $g_{K\Lambda N^*}$, can be extracted from the quark model predictions where the information about the decay amplitude for the $N^* \rightarrow K\Lambda$ decay is given [38]. They are related by the following relation [39]:

$$\langle K(\vec{q}) \Lambda(-\vec{q}, m_f) | -i\mathcal{H}_{\text{int}} | N^*(\mathbf{0}, m_j) \rangle = 4\pi M_{N^*} \sqrt{\frac{2}{|\vec{q}|}} \sum_{\ell, m_\ell} \langle \ell m_\ell \frac{1}{2} m_f | j m_j \rangle Y_{\ell, m_\ell}(\hat{q}) G(\ell), \tag{14}$$

where $\langle \ell m_\ell \frac{1}{2} m_f | j m_j \rangle$ and $Y_{\ell, m_\ell}(\hat{q})$ are the Clebsch-Gordan coefficients and spherical harmonics, respectively. The decay width is then obtained from the partial-wave decay amplitude $G(\ell)$

$$\Gamma(N^* \rightarrow K\Lambda) = \sum_{\ell} |G(\ell)|^2. \tag{15}$$

The spin and parity of the nucleon resonance impose constraints on the relative orbital angular momentum ℓ of the $K\Lambda$ final state. In the case of a $j^P = \frac{1}{2}^-$ resonance, the relative orbital angular momentum is restricted by the angular momentum conservation, so the s wave ($\ell = 0$) is only possible. Similarly, for the resonances of $j^P = (1/2^+, 3/2^+)$, $j^P = (3/2^-, 5/2^-)$, $j^P = (5/2^+, 7/2^+)$, and $j^P = 7/2^-$, the final-particle states are in the relative p , d , f , and g waves, respectively. As a result, the relations between the decay amplitudes and the strong coupling constants for the

decays of the $j^P = (1/2^\pm, 3/2^\pm, 5/2^\pm, 7/2^\pm)$ resonances into the final state are derived as follows:

$$\begin{aligned}
G\left(\frac{1+P}{2}\right) &= \mp \sqrt{\frac{|\vec{q}|(E_\Lambda \mp M_\Lambda)}{4\pi M_{N^*}}} g_{K\Lambda N^*} \text{ for } N^*(1/2^P), \\
G\left(\frac{3-P}{2}\right) &= \pm \sqrt{\frac{|\vec{q}|^3(E_\Lambda \pm M_\Lambda)}{12\pi M_{N^*}}} \frac{g_{K\Lambda N^*}}{M_K} \text{ for } N^*(3/2^P), \\
G\left(\frac{5+P}{2}\right) &= \mp \sqrt{\frac{|\vec{q}|^5(E_\Lambda \mp M_\Lambda)}{30\pi M_{N^*}}} \frac{g_{K\Lambda N^*}}{M_K^2} \text{ for } N^*(5/2^P), \\
G\left(\frac{7-P}{2}\right) &= \pm \sqrt{\frac{|\vec{q}|^7(E_\Lambda \pm M_\Lambda)}{70\pi M_{N^*}}} \frac{g_{K\Lambda N^*}}{M_K^3} \text{ for } N^*(7/2^P),
\end{aligned} \tag{16}$$

where the magnitude of the three-momentum and the energy for the Λ in the rest frame of the resonance are given respectively as

$$|\vec{q}| = \frac{1}{2M_{N^*}} \sqrt{[M_{N^*}^2 - (M_\Lambda + M_K)^2][M_{N^*}^2 - (M_\Lambda - M_K)^2]}, \quad E_\Lambda = \sqrt{M_\Lambda^2 + |\vec{q}|^2}. \tag{17}$$

We should mention that the experimental data on the nucleon resonances in the 2012 edition of Review of Particle Physics [40] were much changed from those in the 2010 edition [41] (see Fig. 2). The $J^P = 5/2^+$ state $F_{15}(2000)$ is split into $N(1860, 5/2^+)$ and $N(2000, 5/2^+)$, whereas the $D_{13}(2080)$ breaks up into $N(1875, 3/2^-)$ and $N(2120, 3/2^-)$. The $S_{11}(2090)$ is changed into $N(1895, 1/2^-)$ and the $N(2060, 5/2^-)$ was previously identified as $D_{15}(2200)$. Since the quark model predictions for the decay amplitudes [38] are obtained from the resonances before the 2012 edition of Review of Particle Physics, we thus make an assumption that the model values can be used for the corresponding revised resonances.

It is worthwhile to compare these coupling constants extracted from the prediction of the quark model [38] with those calculated from the experimental data on the branching ratios [28], although the signs of the couplings can be fixed only in the quark models. In Table II, we summarize both values for the seventeen different nucleon resonances under consideration. Only four resonances provide both of them. Comparing these two values, we find that they are close to each other. Since only the experimental data exist for the $N(1880, 1/2^+)$ and $N(1900, 3/2^+)$, we determine the strong coupling constants for them by using the PDG data. Their signs are determined phenomenologically. The last column in Table II shows the couplings $g_{K\Lambda N^*}$ that are finally determined. They are mostly given within the range of the extracted coupling constants from the quark model predictions [38] or the PDG data [28]. Though we could reproduce the experimental data better by fitting the coupling constants, we have not performed it, because the main concern of the present work lies in understanding the role of each nucleon resonance and we want to avoid additional uncertainties arising from the value of the strong coupling constants.

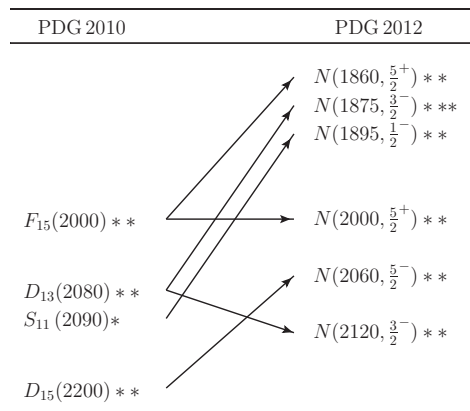


FIG. 2. Change of the N^* spectrum from the 2010 edition of Review of Particle Physics to the 2012 edition.

We can construct the individual amplitudes for the nucleon-resonance exchange using Eqs. (11) and (13) in the

TABLE II. Information on the strong coupling constants of the nucleon resonances. The decay amplitudes $G(\ell)$ [$\sqrt{\text{MeV}}$] are obtained from Ref. [38] and the branching ratios of N^* s to the $K\Lambda$ state are taken from Ref. [28].

State	$G(\ell)$	$g_{K\Lambda N^*}$	$\Gamma_{N^* \rightarrow K\Lambda} / \Gamma_{N^*}$ [%]	$ g_{K\Lambda N^*} $	$g_{K\Lambda N^*}$ (final)
$N(1650, 1/2^-)$	-3.3 ± 1.0	-0.78	5 – 15	0.59 – 1.02	-0.78
$N(1675, 5/2^-)$	0.4 ± 0.3	1.23			1.23
$N(1680, 5/2^+)$	$\simeq 0.1 \pm 0.1$	-2.84			-2.84
$N(1700, 3/2^-)$	-0.4 ± 0.3	2.34			2.34
$N(1710, 1/2^+)$	4.7 ± 3.7	-7.49	5 – 25	4.2 – 9.4	-4.2
$N(1720, 3/2^+)$	-3.2 ± 1.8	-1.80	4 – 5	1.8 – 2.0	-1.1
$N(1860, 5/2^+)$	-0.5 ± 0.3	1.40	seen		1.40
$N(1875, 3/2^-)$	$\simeq 1.7 \pm 1.0$	-2.47	seen		-2.47
$N(1880, 1/2^+)$			12 – 28	4.5 – 6.4	3.0
$N(1895, 1/2^-)$	2.3 ± 2.7	0.34	13 – 23	0.58 – 0.77	0.34
$N(1900, 3/2^+)$			2 – 20	0.53 – 1.7	0.6
$N(1990, 7/2^+)$	$\simeq 1.5 \pm 2.4$	0.61			0.61
$N(2000, 5/2^+)$	-0.5 ± 0.3	0.61			0.61
$N(2060, 5/2^-)$	$\simeq -2.2 \pm 1.0$	-0.52	seen		-0.52
$N(2120, 3/2^-)$	$\simeq 1.7 \pm 1.0$	-1.05			-1.05
$N(2190, 7/2^-)$	$\simeq -1.1$	0.67			0.67
$N(1685, 1/2^+)$					-0.9

form of $\mathcal{M} = I_{N^*} \bar{u}_\Lambda \mathcal{M}_{N^*} u_N$ as in Eq. (5) with $I_{N^*} = 1$:

$$\begin{aligned}
\mathcal{M}_{N^*}^{1/2^\pm} &= \mp g_{K\Lambda N^*} \frac{eh_1}{2M_N} \frac{\Gamma^\pm(q_s + M_{N^*})\Gamma^\mp}{s - M_{N^*}^2 + iM_{N^*}\Gamma_{N^*}} \sigma^{\mu\nu} k_{1\nu} \epsilon_\mu, \\
\mathcal{M}_{N^*}^{3/2^\pm} &= i \frac{g_{K\Lambda N^*}}{M_K} \frac{\Gamma^\mp k_2^\mu}{s - M_{N^*}^2 + iM_{N^*}\Gamma_{N^*}} \Delta_\mu^\rho(q_s) \left[\frac{eh_1}{2M_N} \Gamma_\lambda^\pm \mp \frac{eh_2}{(2M_N)^2} \Gamma^\pm p_{1\lambda} \right] (k_{1\rho} \epsilon^\lambda - k_1^\lambda \epsilon_\rho), \\
\mathcal{M}_{N^*}^{5/2^\pm} &= i \frac{g_{K\Lambda N^*}}{M_K^2} \frac{\Gamma^\pm k_2^\mu k_2^\nu}{s - M_{N^*}^2 + iM_{N^*}\Gamma_{N^*}} \Delta_{\mu\nu}^{\rho\sigma}(q_s) \left[\frac{eh_1}{(2M_N)^2} \Gamma_\lambda^\mp \pm \frac{eh_2}{(2M_N)^3} \Gamma^\mp p_{1\lambda} \right] k_{1\sigma} (k_{1\rho} \epsilon^\lambda - k_1^\lambda \epsilon_\rho), \\
\mathcal{M}_{N^*}^{7/2^\pm} &= i \frac{g_{K\Lambda N^*}}{M_K^3} \frac{\Gamma^\mp k_2^\mu k_2^\nu k_2^\alpha}{s - M_{N^*}^2 + iM_{N^*}\Gamma_{N^*}} \Delta_{\mu\nu\alpha}^{\rho\sigma\delta}(q_s) \left[\frac{eh_1}{(2M_N)^3} \Gamma_\lambda^\pm \pm \frac{eh_2}{(2M_N)^4} \Gamma^\pm p_{1\lambda} \right] k_{1\sigma} k_{1\delta} (k_{1\rho} \epsilon^\lambda - k_1^\lambda \epsilon_\rho), \quad (18)
\end{aligned}$$

where Γ_{N^*} designates the full decay width of N^* . The spin-3/2, -5/2, and -7/2 projection operators, given by Δ_μ^ρ , $\Delta_{\mu\nu}^{\rho\sigma}$, and $\Delta_{\mu\nu\alpha}^{\rho\sigma\delta}$, respectively, are represented in the Rarita-Schwinger formalism [42–45] as in Refs. [34, 35, 46, 47]. The phase factors of the invariant amplitudes for the nucleon resonances cannot be determined by symmetries only, so we regard them as free parameters. These amplitudes are thus written by

$$\mathcal{M}_{\text{Res}} = \sum_{N^*} e^{i\psi_{N^*}} \mathcal{M}_{N^*} F_{N^*}(s), \quad (19)$$

where the gaussian form factor is employed [48, 49]

$$F_{N^*}(q_s^2) = \exp \left\{ -\frac{(q_s^2 - M_{N^*}^2)^2}{\Lambda_{N^*}^4} \right\}. \quad (20)$$

3. Before we present the numerical results, we need to mention how the model parameters are fixed. The cutoff masses are fixed to be $\Lambda_{B(N,\Lambda,\Sigma),N^*} = 0.9$ GeV for simplicity. We do not fit the values of the cutoff masses to avoid additional uncertainties arising from them. We find that at high energies above the CM energy $W = 2.2$ GeV, where K^* Reggeon exchange comes into a dominant play, the rotating Regge phase ($e^{-i\pi\alpha_{K^*}(t)}$) and the phase angle $\psi_{N^*} = \pi$ turn out to be the best choice.

In the left panel of Fig. 3, the total cross section for the $\gamma n \rightarrow K^0\Lambda$ reaction is drawn as a function of the CM energy. The N^* contributions are dominant in the lower-energy region ($W \lesssim 2.2$ GeV). K^* Reggeon exchange in the t channel being included, the result is in agreement with the CLAS data [26]. As W increases, the K^* Reggeon takes over N^* contributions. Because of K^* Reggeon exchange, the total cross section behaves asymptotically as $\sigma \sim s^{\alpha_{K^*}(0)-1}$ and describes the experimental data well. As shown in the left panel of Fig. 3, the result is slightly underestimated in the vicinity of the threshold energy, compared to the CLAS data. Each contribution of various nucleon resonances is drawn in the right panel of Fig. 3. The well-known $N(1650, 1/2^-)$ and $N(1720, 3/2^+)$ are the

most dominant ones. While the $N(1675, 5/2^-)$, $N(1710, 1/2^+)$, $N(1880, 1/2^+)$, $N(1900, 3/2^+)$, $N(1990, 7/2^+)$, and $N(2120, 3/2^-)$ have sizable effects on the total cross section, all other resonances almost do not affect it, so we show only the contributions of the nine nucleon resonances in the figure. Moreover, the $N(1685, 1/2^+)$ resonance has only a marginal effect on the total cross section. Thus, as far as the results of the total cross section are concerned, the present ones are more or less similar to those of Ref. [50] where the Bonn-Gatchina coupled-channel partial-wave analysis was used. In Ref. [50], it was shown that the partial waves $J^P = 1/2^\pm$ and $3/2^+$ contribute dominantly to the total cross section and the narrow bump structure is not seen unlike the $\gamma n \rightarrow \eta n$ cross section. However, the inclusion of the $N(1685, 1/2^+)$ improves the data around $W = 1.68$ GeV in the present calculation.

Figure 4 draws the differential cross sections for the $\gamma n \rightarrow K^0 \Lambda$ reaction as a function of $\cos \theta_{\text{CM}}^{K^0}$, being compared with the FOREST experimental data [25]. The photon energy is varied from $E_\gamma = 937.5$ MeV to $E_\gamma = 1137.5$ MeV. The dashed curve is drawn for the contribution of K^* Reggeon exchange. As expected, its effect is rather small in the range of the photon energy given in Fig. 4. Here, main interest lies in the effect of the narrow resonance $N(1685, 1/2^+)$. While the dotted curve is depicted without the $N(1685, 1/2^+)$ taken into account, the solid one includes it. Though the effect of the $N(1685, 1/2^+)$ is very small at smaller values of E_γ , it comes into play as E_γ increases. In particular, the experimental data of the differential cross section at $E_\gamma = 1037.5$ MeV and $E_\gamma = 1062.5$ MeV can be explained only by including the narrow resonance $N(1685, 1/2^+)$. Otherwise, the results would be overestimated in the forward direction and would be underestimated in the backward direction. Although the $N(1685, 1/2^+)$ does not give any significant contribution to the total cross section, it is essential to consider it to explain the differential cross section data in the range of the photon energies $1037 \text{ MeV} \leq E_\gamma \leq 1062 \text{ MeV}$.

In Fig. 5, we compare the present results of the differential cross section with the CLAS data [26]. The CLAS experiment covers a much wider range of the photon energies ($0.97 \text{ GeV} \leq E_\gamma \leq 2.45 \text{ GeV}$) than the FOREST experiment. The first three figures in the first row of Fig. 5 can be compared to the FOREST data given in Fig. 4. Though there are some discrepancies between these two experimental data, general tendency of the data is similar each other. The present results are also in qualitative agreement with the CLAS data. In particular, the narrow resonance $N(1685, 1/2^+)$ pulls down the differential cross section at $E_\gamma = 1.05$ GeV in the forward direction. On the other hand, the $N(1685, 1/2^+)$ makes it enhanced in the backward direction, as we already discussed in Fig. 4. As a result, the inclusion of the $N(1685, 1/2^+)$ provides noticeably better agreement with the data. As E_γ increases, i.e. $E_\gamma \geq 1.8$ GeV (or $W \geq 2.05$ GeV), the results are in good agreement with the CLAS data. This can be understood by K^* Reggeon exchange which governs the $\gamma n \rightarrow K^0 \Lambda$ process in the higher energy region.

We want to mention that we fit the value of the $K \Lambda N(1685)$ coupling constant to be $g_{K \Lambda N(1685)} = -(0.8 - 1.1)$, which implies the branching ratio $\text{Br}(N(1685, 1/2^+) \rightarrow K \Lambda) = (0.5 - 1.0)\%$ with $\Gamma_{N(1685, 1/2^+)} = 30$ MeV. Consequently, we get the partial decay width $\Gamma_{N^* \rightarrow K \Lambda}$ to be $(0.15 - 0.30)$ MeV, whereas another theoretical analysis based on the soliton picture yields 0.7 (1.56) MeV for $M_{N^*} = 1680$ (1730) MeV [51]. We hope that future experiments may clarify these predictions. Meanwhile, Ref. [50] obtained the following upper limit

$$\sqrt{\text{Br}(N(1685) \rightarrow K \Lambda)} A_{N^*}^{\text{total}} < 6 \times 10^{-3} \text{ GeV}^{-1/2} \quad (21)$$

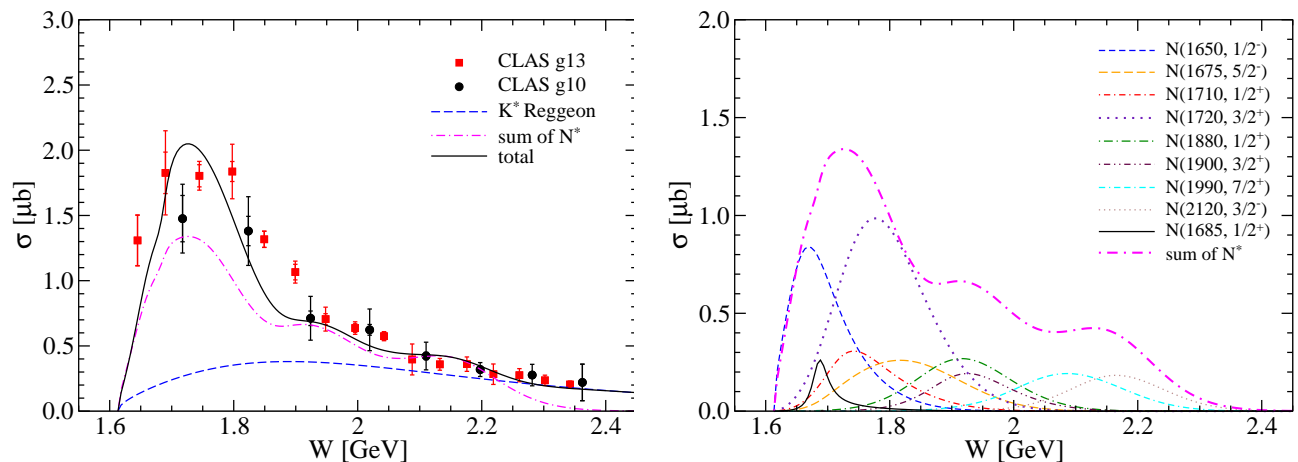


FIG. 3. Left: Total cross section for the $\gamma n \rightarrow K^0 \Lambda$ reaction as a function of the CM energy. The dashed (blue), dot-dashed (magenta), and solid (black) curves correspond to contribution from K^* Reggeon exchange, that from the sum of N^* exchanges, and the total contribution, respectively. The data are taken from the CLAS experiment [26]. Right: Each contribution to $\gamma n \rightarrow K^0 \Lambda$ reaction for various nucleon resonances.

which is consistent with our result, i.e., $(3.7 - 5.2) \times 10^{-3} \text{ GeV}^{-1/2}$.

We have fixed the mass of this narrow resonance to be $M_{N^*} = 1685 \text{ MeV}$. On the other hand, a simultaneous analysis of the $\gamma p \rightarrow K^+ \Lambda$ and $\gamma n \rightarrow K^0 \Lambda$ channels finds that the most appropriate mass is 1650 MeV [21, 22]. The energies at $E_\gamma = 0.97$ and 1.05 GeV in Fig. 5 correspond approximately to the energies at $W = 1650$ and 1685 MeV , respectively. Thus, selecting such a low mass $M_{N^*} = 1650 \text{ MeV}$ is not suitable to describe the CLAS data in our calculation, since the inclusion of the narrow resonance greatly improves the cross section result at the energy $E_\gamma = 1.05 \text{ GeV}$.

Figure 6 draws the differential cross sections for the $\gamma n \rightarrow K^0 \Lambda$ reaction as a function of the CM energy with $\cos \theta_{\text{CM}}^{K^0}$ fixed. As in the case of Fig. 5, including the narrow resonance $N(1685, 1/2^+)$ improves the description of the CLAS data near the threshold region [26]. In particular, the $N(1685, 1/2^+)$ enhances the differential cross section in the backward angle, i.e. in the range of $-0.7 < \cos \theta_{\text{CM}}^{K^0} < 0.0$ around $W = 1.68 \text{ GeV}$. On the other hand, the $N(1685, 1/2^+)$ makes it reduced in the forward direction. Yet another noticeable feature is that, by the inclusion of the $N(1685, 1/2^+)$, destructive effects between it and other resonances begin to appear at the corresponding pole position as the angle $\cos \theta$ increases as clearly seen in the last row of Fig. 6. This tendency is also shown in the CLAS data, especially in the g10 ones. This can strongly support the evidence of the existence of the narrow resonance $N(1685, 1/2^+)$ in $K^0 \Lambda$ photoproduction. One cannot explain these dip structures merely by adjusting the model parameters of other resonances.

It is of great importance to examine the beam asymmetry and other polarization observables of $K^0 \Lambda$ photoproduction both experimentally and theoretically, since they can clarify more clearly the role of nucleon resonances. In Fig. 7, we draw the predictions of the beam asymmetry $\Sigma_{\gamma n \rightarrow K^0 \Lambda}$ as a function of $\cos \theta$ for four different beam energies. The beam asymmetry is defined as follows:

$$\Sigma_{\gamma n \rightarrow K^0 \Lambda} = \frac{\frac{d\sigma}{d\Omega}_\perp - \frac{d\sigma}{d\Omega}_\parallel}{\frac{d\sigma}{d\Omega}_\perp + \frac{d\sigma}{d\Omega}_\parallel}, \quad (22)$$

where the subscript \perp means that the photon polarization vector is perpendicular to the reaction plane whereas \parallel denotes the parallel photon polarization to it. The left panel of Fig. 7 depicts the results of the beam asymmetry without the nu' However, it falls off drast the beam

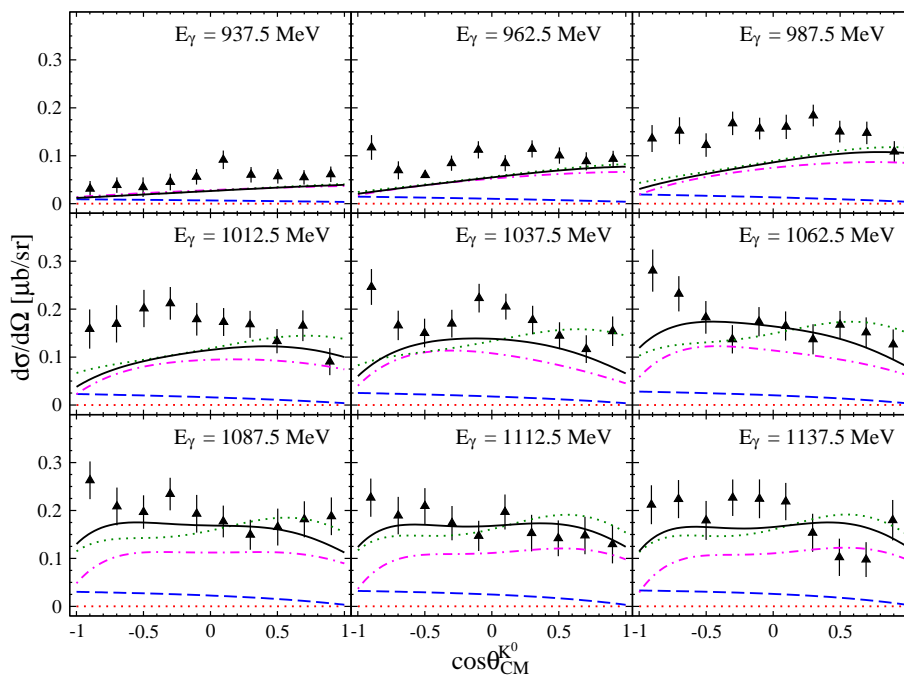


FIG. 4. Differential cross section for the $\gamma n \rightarrow K^0 \Lambda$ reaction as a function of $\cos \theta_{\text{CM}}^{K^0}$ for each beam energy. The dashed (blue), dot-dashed (magenta), and solid (black) curves correspond to the contribution from K^* Reggeon exchange, that from the sum of N^* exchanges, and the total contribution, respectively. The dotted (green) one indicates the total contribution without the effect of the narrow resonance $N(1685, 1/2^+)$. The data are taken from the FOREST experiment [25].

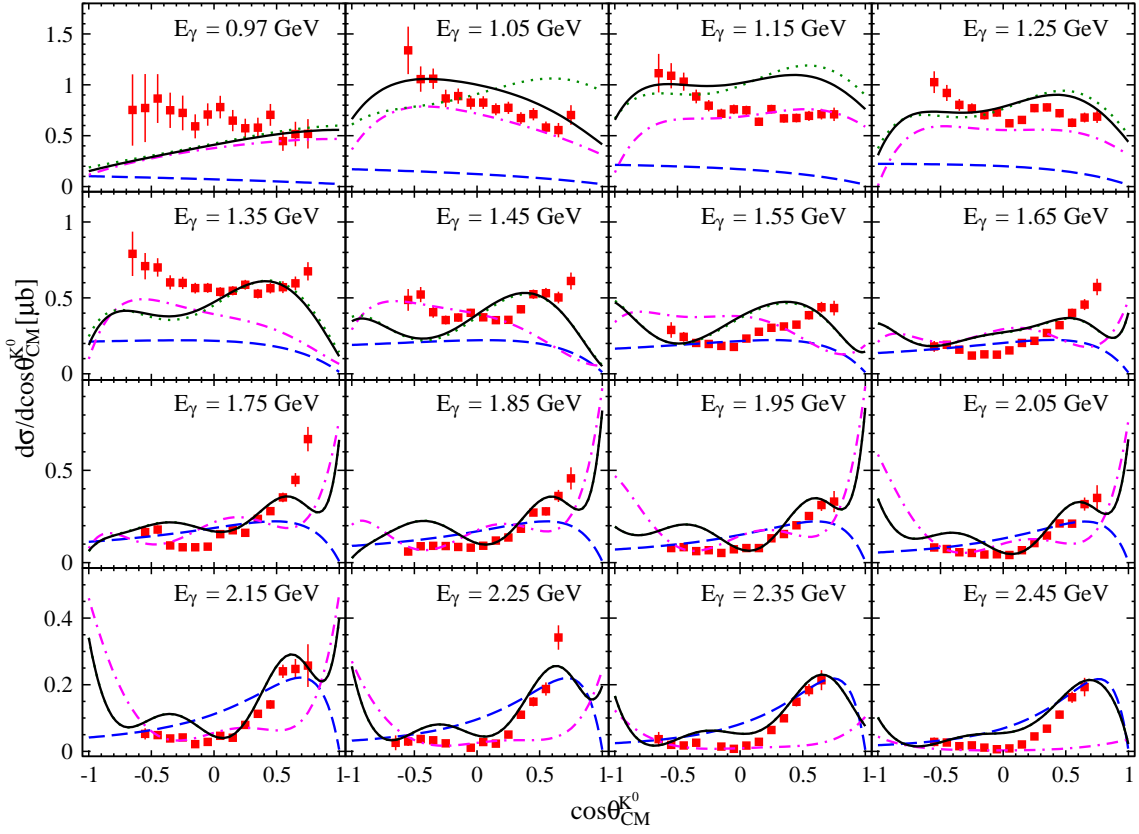


FIG. 5. Differential cross section for the $\gamma n \rightarrow K^0 \Lambda$ reaction as a function of $\cos \theta_{\text{CM}}^{K^0}$ for each beam energy. The notations are the same as in Fig. 4. The data are taken from the CLAS experiment [26].

asymmetry become larger. On the other hand, when the nucleon resonances are included, the structure of the beam asymmetry is entirely changed. At $E_\gamma = 1.05$ GeV, the $\cos \theta$ dependence of Σ_γ is opposite to the case without the nucleon resonances, that is, when $\cos \theta$ increases, the beam asymmetry increases till around $\cos \theta = -0.3$ and then slowly falls off. However, if one increase the photon energy, the results of Σ_γ are changed dramatically. One can understand this interesting feature of Σ_γ . Each contribution of the nucleon resonances depends on E_γ . As E_γ increases, higher lying nucleon resonances comes into play. It brings about the remarkable changes of the beam asymmetry.

4. In the present work, we investigated $K^0 \Lambda$ photoproduction, aiming at understanding the nature of the narrow resonance structure around 1.68 GeV. We employed an effective Lagrangian method combined with a Regge approach. We included seventeen different nucleon resonances in the s channel together with nucleon exchange as a background. In addition, we considered Λ and Σ exchanges the u channel. In the t channel, we included K^* Reggeon exchange which governs the behavior of the $\gamma n \rightarrow K^0 \Lambda$ amplitude in higher energy regions. Since charged kaon photoproduction has been widely investigated in the literature, it is of great interest to compare the role of each diagram in both the charged and neutral productions. Even though the photocouplings are different, the important contributions in the s channel are similar to each other. For example, in Refs. [48, 49, 52–54], the $N(1650, 1/2^-)$ and $N(1720, 3/2^+)$ are the most significant ones and the $N(1900, 3/2^+)$ is also required for the description of the cross section data.

We have taken into account the nucleon resonances which appeared only in the PDG data. We were able to reproduce the recent CLAS and FOREST data reasonably well without any complicated fitting procedure, even though the nucleon resonances from the PDG data are considered only. The sign ambiguities of the strong coupling constants for the nucleon resonances were resolved by relating them to information on the partial-wave decay amplitudes predicted by a quark model. We found that the narrow nucleon resonance $N(1685, 1/2^+)$ has a certain contribution to the differential cross sections near the threshold energy. It enhances them in the backward direction while it makes them decreased in the forward direction, whereas it is difficult to see the effect of the $N(1685, 1/2^+)$ on the total cross section. It is interesting to extend our approach to the study of $K\Sigma$ photoproduction [55] and $K\Lambda(K\Sigma)$ electroproduction [56].

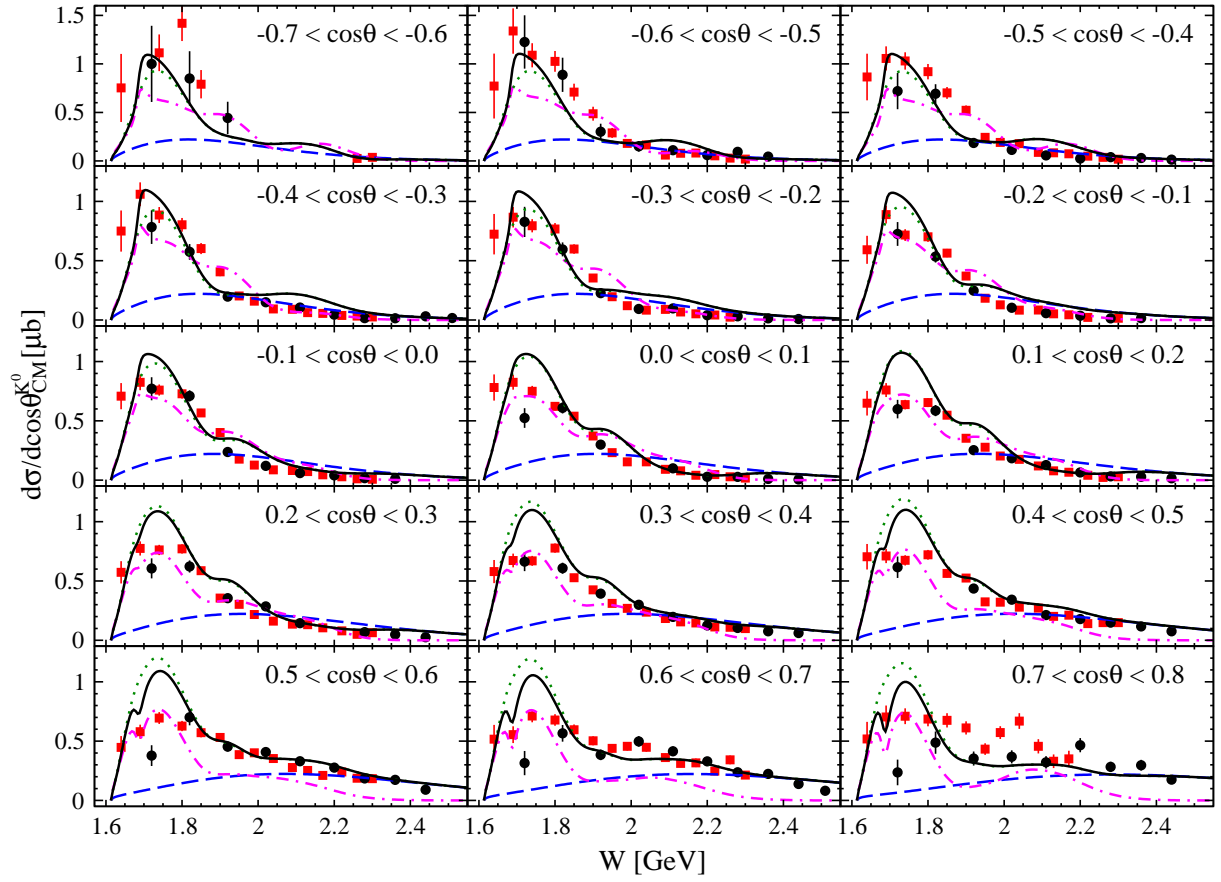


FIG. 6. Differential cross section for $\gamma n \rightarrow K^0 \Lambda$ as a function of W for each $\cos \theta_{\text{CM}}^{K^0}$. The notations are the same as Fig. 4. The data are taken from the CLAS experiment [26].

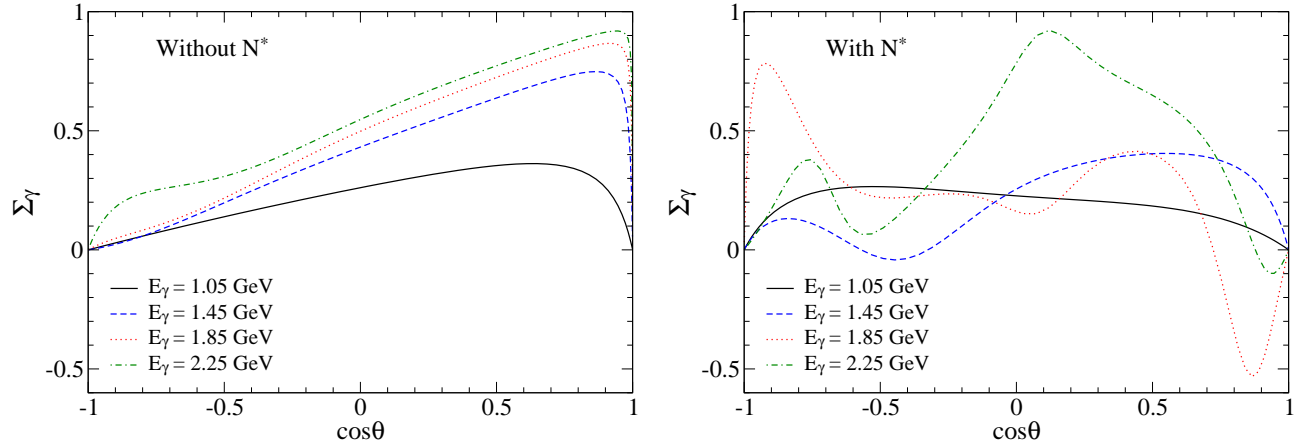


FIG. 7. Beam asymmetry $\Sigma_{\gamma n \rightarrow K^0 \Lambda}$ as a function of $\cos \theta$ for each beam energy when the nucleon resonances are not included (Left) and included (Right), respectively.

Relevant works will appear elsewhere.

ACKNOWLEDGMENTS

Authors are grateful to N. Compton for providing us with the CLAS experimental data. They want to express the gratitude to T. Ishikawa, Y. Tsuchikawa, H. Shimizu, Y. Oh, and Gh.-S. Yang for fruitful discussions. H.-Ch. K. is grateful to A. Hosaka, T. Maruyama, M. Oka for useful discussions. He wants to express his gratitude to the members of the Advanced Science Research Center at Japan Atomic Energy Agency for the hospitality, where part of the present work was done. S.H.K. acknowledges support by the Ministry of Science, ICT & Future Planning, Gyeongsangbuk-do and Pohang City. This work was supported by the National Research Foundation of Korea (NRF) grant funded by the Korea government(MSIT) (No. 2018R1A5A1025563).

-
- [1] V. Kuznetsov *et al.*, GRAAL Collaboration, Phys. Lett. B **647** (2007) 23.
 - [2] F. Miyahara *et al.*, Prog. Theor. Phys. Suppl. **168** (2007) 90.
 - [3] I. Jaegle *et al.*, CBELSA and TAPS Collaborations, Phys. Rev. Lett. **100** (2008) 252002.
 - [4] D. Werthmüller *et al.*, A2 Collaboration, Phys. Rev. Lett. **111** (2013) 232001.
 - [5] D. Werthmüller *et al.*, A2 Collaboration, Phys. Rev. C **90** (2014) 015205.
 - [6] L. Witthauer *et al.*, A2 Collaboration, Phys. Rev. Lett. **117** (2016) 132502.
 - [7] D. Diakonov, V. Petrov, M. V. Polyakov, Z. Phys. A **359** (1997) 305.
 - [8] M. V. Polyakov, A. Rathke, Eur. Phys. J. A **18** (2003) 691.
 - [9] H.-Ch. Kim, M. Polyakov, M. Praszalowicz, G. S. Yang, K. Goeke, Phys. Rev. D **71** (2005) 094023.
 - [10] G. S. Yang, H.-Ch. Kim, PTEP **2013** (2013) 013D01.
 - [11] G. S. Yang, H.-Ch. Kim, in preparation (2018).
 - [12] A. V. Anisovich, E. Klempt, B. Krusche, V. A. Nikonov, A. V. Sarantsev, U. Thoma, D. Werthmüller, Eur. Phys. J. A **51** (2015) 72.
 - [13] A. V. Anisovich, V. Burkert, E. Klempt, V. A. Nikonov, A. V. Sarantsev, U. Thoma, Phys. Rev. C **95** (2017) 035211.
 - [14] V. Kuznetsov *et al.*, JETP Lett. **105** (2017) 625.
 - [15] K. S. Choi, S. i. Nam, A. Hosaka, H.-Ch. Kim, Phys. Lett. B **636** (2006) 253.
 - [16] V. Shklyar, H. Lenske, U. Mosel, Phys. Lett. B **650** (2007) 172.
 - [17] A. Fix, L. Tiator, M. V. Polyakov, Eur. Phys. J. A **32** (2007) 311.
 - [18] R. A. Arndt, W. J. Briscoe, M. W. Paris, I. I. Strakovsky, R. L. Workman, Chin. Phys. C **33** (2009) 1063.
 - [19] M. Döring, K. Nakayama, Phys. Lett. B **683** (2010) 145.
 - [20] T. Mart, Phys. Rev. C **83** (2011) 048203.
 - [21] T. Mart, Phys. Rev. D **83** (2011) 094015.
 - [22] T. Mart, Phys. Rev. D **88** (2013) 057501.
 - [23] T. Mart, A. Rusli, PTEP **2017** (2017) 123D04.
 - [24] Y. Tsuchikawa *et al.*, JPS Conf. Proc. **10** (2016) 032010.
 - [25] Y. Tsuchikawa *et al.*, JPS Conf. Proc. **17** (2017) 062007.
 - [26] N. Compton *et al.*, CLAS Collaboration, Phys. Rev. C **96** (2017) 065201.
 - [27] D. H. Ho *et al.*, CLAS Collaboration, arXiv:1805.04561 [nucl-ex].
 - [28] M. Tanabashi *et al.*, Particle Data Group, Phys. Rev. D **98** (2018) 030001.
 - [29] V. G. J. Stoks, Th. A. Rijken, Phys. Rev. C **59** (1999) 3009; Th. A. Rijken, V. G. J. Stoks, Y. Yamamoto, *ibid.* **59** (1999) 21.
 - [30] T. Vrancx, L. De Cruz, J. Ryckebusch, P. Vancraeyveld, Phys. Rev. C **84** (2011) 045201.
 - [31] J. Kristiano, S. Clymton, T. Mart, Phys. Rev. C **96** (2017) 052201(R).
 - [32] A. Donnachie, H. G. Dosch, P. V. Landshoff, O. Nachtmann, Pomeron Physics and QCD (Cambridge University Press, UK, 2002).
 - [33] M. Guidal, J. M. Laget, M. Vanderhaeghen, Nucl. Phys. A **627** (1997) 645.
 - [34] Y. Oh, J. Korean Phys. Soc. **59** (2011) 3344.
 - [35] Y. Oh, C. M. Ko, K. Nakayama, Phys. Rev. C **77** (2008) 045204.
 - [36] C. Patrignani *et al.*, Particle Data Group, Chin. Phys. C **40** (2016) 100001.
 - [37] G.-S. Yang, Ph.D. thesis, Bochum Univeristy, 2010.
 - [38] S. Capstick, W. Roberts, Phys. Rev. D **58** (1998) 074011.
 - [39] S. H. Kim, S. i. Nam, D. Jido, H.-Ch. Kim, Phys. Rev. D **96** (2017) 014003.
 - [40] J. Beringer *et al.*, Particle Data Group, Phys. Rev. D **86** (2012) 010001.
 - [41] K. Nakamura *et al.*, Particle Data Group, J. Phys. G **37** (2010) 075021.
 - [42] R. E. Behrends, C. Fronsdal, Phys. Rev. **106** (1957) 345.
 - [43] J. G. Rushbrooke, Phys. Rev. **143** (1966) 1345.
 - [44] S. J. Chang, Phys. Rev. **161** (1967) 1308.
 - [45] F. A. Berends, J. W. van Holten, P. van Nieuwenhuizen, B. de Wit, Nucl. Phys. B **154** (1979) 261.
 - [46] S. H. Kim, S. i. Nam, Y. Oh, H.-Ch. Kim, Phys. Rev. D **84** (2011) 114023.

- [47] S. H. Kim, S. i. Nam, A. Hosaka, H.-Ch. Kim, Phys. Rev. D **88** (2013) 054012.
- [48] T. Corthals, J. Ryckebusch, T. Van Cauteren, Phys. Rev. C **73** (2006) 045207.
- [49] L. De Cruz, J. Ryckebusch, T. Vranckx, P. Vancraeyveld, Phys. Rev. C **86** (2012) 015212.
- [50] A. V. Anisovich *et al.*, Phys. Rev. C **96** (2017) 055202.
- [51] R. A. Arndt, Y. I. Azimov, M. V. Polyakov, I. I. Strakovsky, R. L. Workman, Phys. Rev. C **69** (2004) 035208.
- [52] V. Shklyar, H. Lenske, U. Mosel, Phys. Rev. C **72** (2005) 015210.
- [53] R. A. Schumacher, M. M. Sargsian, Phys. Rev. C **83** (2011) 025207.
- [54] T. Mart, S. Sakinah, Phys. Rev. C **95** (2017) 045205.
- [55] P. Aguar-Bartolome *et al.*, A2 Collaboration, Phys. Rev. C **88** (2013) 044601.
- [56] D. S. Carman *et al.*, CLAS Collaboration, Phys. Rev. C **87** (2013) 025204.